Chemically Mediated Mechanical Expansion of the Pollen Tube Cell Wall

Enrique R. Rojas,[†*] Scott Hotton,[‡] and Jacques Dumais[‡]
[†]Department of Physics and [‡]Department of Organismic and Evolutionary Biology, Harvard University, Cambridge, Massachusetts

ABSTRACT Morphogenesis of plant cells is tantamount to the shaping of the stiff cell wall that surrounds them. To this end, these cells integrate two concomitant processes: 1), deposition of new material into the existing wall, and 2), mechanical deformation of this material by the turgor pressure. However, due to uncertainty regarding the mechanisms that coordinate these processes, existing models typically adopt a limiting case in which either one or the other dictates morphogenesis. In this report, we formulate a simple mechanism in pollen tubes by which deposition causes turnover of cell wall cross-links, thereby facilitating mechanical deformation. Accordingly, deposition and mechanics are coupled and are both integral aspects of the morphogenetic process. Among the key experimental qualifications of this model are: its ability to precisely reproduce the morphologies of pollen tubes; its prediction of the growth oscillations exhibited by rapidly growing pollen tubes; and its prediction of the observed phase relationships between variables such as wall thickness, cell morphology, and growth rate within oscillatory cells. In short, the model captures the rich phenomenology of pollen tube morphogenesis and has implications for other plant cell types.

INTRODUCTION

Cellular morphogenesis is the complex process by which cells attain their functional shapes. In this context, cells—including those of plants, fungi, bacteria, and many protists—that are enclosed in cell walls are remarkable in two respects:

1. Many-walled cells are capable of massive growth and, equivalently, vast cell wall expansion. For example, between germination and maturity, an angiosperm pollen tube (Fig. 1 *A*) may increase its surface area by a factor of 10^5.
2. The polymeric cell wall, which defines the cell's shape, is an intrinsically stiff structure; consequently, morphogenesis for these cells requires the generation of extreme forces.

These facts underscore the two processes that are essential to the morphogenesis of walled cells: secretory exocytosis (deposition) of wall polymers and turgor-driven deformation of this material.

The topic of this article is the relationship between deposition and mechanics in plant cells. We are guided by three outstanding questions: First, what is the constitutive rheological behavior of the cell wall? Second, how, if at all, does deposition affect the rheological properties of the wall? Third, how is deposition balanced with mechanical expansion such that wall thickening due to the former precisely equals wall thinning due to the latter? These questions have remained largely unresolved, though experiments have provided a rich phenomenology from which to draw insight.

The rheological behavior of the cell wall results from its microscopic architecture. The plant cell wall is primarily composed of three polysaccharides: pectin, cellulose, and hemicellulose. Irreversible mechanical deformation of this material requires a mechanism for dissipation of elastic energy. Ray and Ruesink considered two possibilities: 1), that the wall is essentially a viscous liquid, albeit with an extremely high viscosity; and 2), that the wall is a single cross-linked macromolecule and that irreversible deformation results from dissociation of load-bearing cross-links (1). This second possible mechanism was termed a "chemorheological process" because, according to it, the effective viscosity of the wall is determined by a chemical reaction. Experimentally, the rapid change of the growth rate of plant tissue in response to variations in temperature supports the chemorheological conception, and the magnitude of this response suggests that the chemistry associated with cross-link dissociation is rate-limited by enzyme kinetics (1).

Recent evidence corroborates the chemorheological conception by demonstrating that the rate of dissociation of pectin cross-links regulates the growth rate of the alga *Chara corallina* (2). Although the cellulose-hemicellulose network is also an important determinant of wall rheology (3), the relative contributions of the pectin and cellulose-hemicellulose networks to the gross mechanical properties of the wall is still a matter of debate.

The fungal metabolite brefeldin A, which interferes with the plant cell secretory pathway, has been used to study the effects of deposition on the wall's rheological properties. Diminishing or depleting deposition with brefeldin A not only inhibits growth (4,5), but also increases the effective viscosity of the wall (4). Deposition apparently has the effect of softening the wall, thereby allowing turgor to deform it.

Submitted April 5, 2011, and accepted for publication August 2, 2011.

*Correspondence: errojas@post.harvard.edu

Editor: Douglas Nyle Robinson.

0006-3495/11/10/1844/10 $2.00

doi: 10.1016/j.bpj.2011.08.016

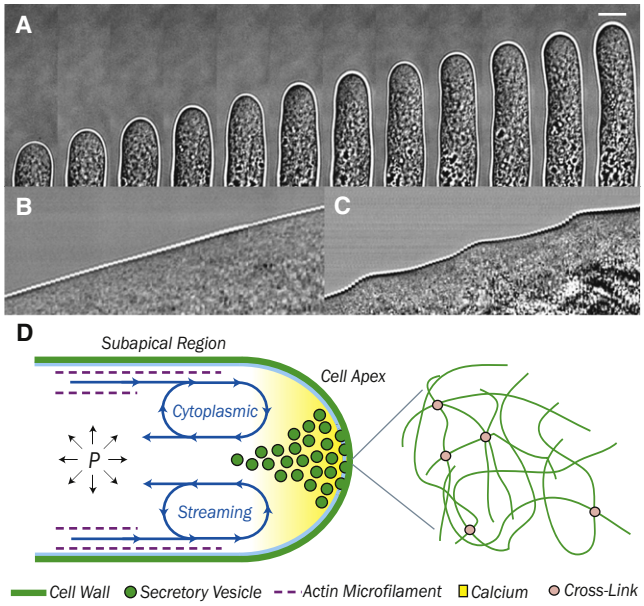

FIGURE 1 (*A*) Pollen tubes exhibit tip growth morphogenesis. (Scale bar = 10 μm, Δt between images = 6 s.) Kymographs of pollen tubes illustrate how this process can be either (*B*) steady or (*C*) oscillatory (elapsed time in kymographs is 6 min). Lily pollen tubes oscillate with periods between 20 and 120 s. (*D*) The physical elements of pollen-tube morphogenesis.

The most striking demonstration of the ability of plants to balance deposition with mechanical thinning is perhaps the phenomenon of stored growth. It is well understood that plasmolysis (depletion of turgor) inhibits the growth of plant cells. Under certain circumstances, reestablishing the turgor after plasmolysis induces a period of rapid wall expansion during which the cell or tissue grows to the same size that it would have attained had it not been plasmolyzed (6–9). It has been suggested that this phenomenon relies on a reservoir of wall material being deposited during plasmolysis, effectively being stored for rapid expansion, pending repressurization (9). Indeed, in pollen tubes as well as root hairs, plasmolysis does not affect deposition and results in the buildup of a thick cell wall (10,11).

THE POLLEN TUBE

The pollen tube has become a fruitful model system in the field of plant cell morphogenesis. These cells are ideal for experiment because they are naturally isolated from tissue and because they employ tip growth—i.e., rapid cell wall expansion that is confined to the cell apex. As compared with the uniform wall expansion of diffusely growing cells, wall expansion during tip growth is, de facto, inhomogeneous (variable in space), making tip-growing cells useful systems for studying the factors that regulate expansion rates. The observations of both steady growth (i.e., constant elongation rate; see Fig. 1 *B* and see Movie S1 in the Supporting Material) and oscillatory growth (12,13) (Fig. 1 *C* and see Movie S2) have further enriched the study of pollen tubes. Within oscillatory cells, in addition to the elongation rate, a host of other measurable quantities (e.g., wall thickness (10), cytoplasmic concentrations of enzymes (14,15), and calcium (13,16,17)) oscillate, each with a distinct phase. These cells, then, are natural probes of the dynamical feedback system that governs plant cell morphogenesis. Finally, because the expanding region of the pollen tube wall of some species is devoid of cellulose (18), these cells offer the unique opportunity to study the mechanical properties of pectin, in vivo, and isolated from the cellulose-hemicellulose network.

Fig. 1 *D* shows the subcellular structures that are implicated in the control of deposition and mechanical deformation of the pollen tube wall. Deposition depends on the delivery of secretory vesicles to the apical plasma membrane from the subapical region of the cell, where the Golgi body packages them with pectin. This transport is mediated by myosin motors, which tow vesicles along longitudinal actin microfilaments (19). The actin cytoskeleton, however, extends only to the base of the apex (20,21). Thus, vesicles are presumed to complete their journey passively, either by diffusion or by viscous entrainment with cytoplasmic streaming (22). An apical cytosolic calcium gradient is maintained in part by calcium influx through transmembrane stretch-activated channels, and may be involved in regulating actin polymerization and/or determining polarity (23).

At the molecular scale, pectin forms an amorphous, cross-linked hydrogel (24). For such a gel, the lengths of polymer bridging two cross-links act as entropic springs and stretch elastically in response to forces in the network (25).

MODELING MORPHOGENESIS

Because of their simple geometry, pollen tubes and other tip-growing cells (such as root hairs and fungal hyphae) have inspired numerous mathematical models. These studies have succeeded in capturing cell morphology by explicitly prescribing either the spatial profile of the deposition rate (26), the profile of wall viscosity (27–29), or both (30). Although these top-down models do not couple deposition and mechanics, in some instances they yield useful predictions concerning the nature of the cell's deposition machinery (26,30). By addressing the feedback between cell elongation and deposition, Kroeger et al. (31,32) were able to demonstrate oscillatory dynamics in pollen tubes.

Mathematical models of diffusely growing cells have typically ignored the role of deposition and focused on the rheological properties of the cell wall, following either the viscous conception (33) or the chemorheological conception (34). The latter model is able to capture more experimentally observed phenomena, in particular the response of cell growth rate to changes in turgor pressure.

In light of these efforts, the goal here is to resolve the mechanism by which deposition and mechanical deformation

conspire to produce continuous expansion in the case of the pectic cell wall of lily pollen tubes. To do this we construct a bottom-up model of pollen tube morphogenesis based on a simple concept: that deposition chemically loosens the wall by breaking load-bearing cross-links while simultaneously creating new, load-free cross-links, thereby effecting a fail-safe scenario for mechanical expansion. The data we provide herein combined with the wealth of data from the pollen tube literature are highly constraining and allow us to test our model much more rigorously than would measurements of cell shape and/or behavior alone.

A MECHANISM FOR WALL EXPANSION

Before constructing the model, it is useful to define a coordinate system with respect to the geometry of the pollen tube wall. The cell surface can be conveniently parameterized by the arclength from the pole of the cell, s, and the azimuthal angle, θ (Fig. 2) (28). We refer to these as the "meridional" and "circumferential" directions, respectively. Moreover, given the axial symmetry of the cell, any spatially dependent quantity is a function only of s.

The pollen-tube growth cycle nominally begins with the deposition of new pectin into the cell wall (Fig. 3, Steps 1 and 2; see the Supporting Material for a detailed derivation of the dynamical system described previously). Pectin is mostly composed of methyl-esterified poly-galacturonan, which can be de-esterified by the enzyme pectin methylesterase (PME; Fig. 3, Step 3) (35). Two (negatively charged) de-esterified residues can then form a cross-link by binding a single divalent calcium ion (Fig. 3, Step 4) (24). In pollen tubes, esterified pectins are found exclusively in the apical cell wall whereas de-esterified and cross-linked pectins are found throughout the wall (36,37). That is, nascent pectin is deposited in an esterified form at the cell apex and is subsequently de-esterified and cross-linked. Because the

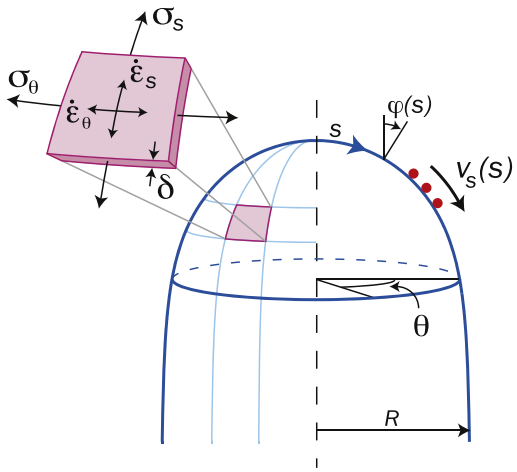

FIGURE 2 Parameterization of the cell surface.

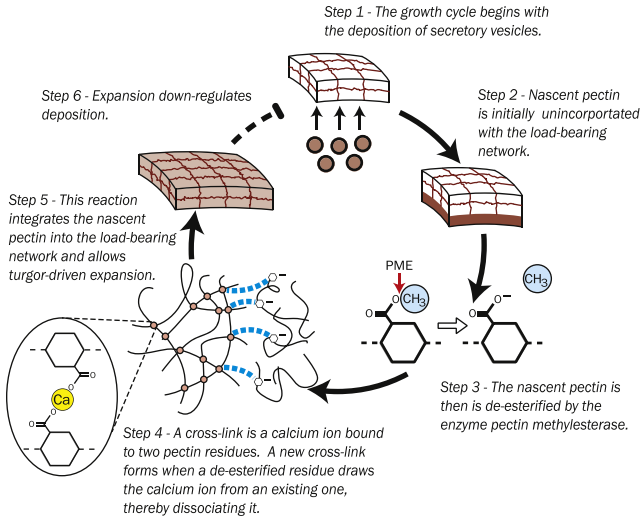

FIGURE 3 Feedback system between the key processes of pollen-tube cell wall expansion.

PME distribution in the wall is roughly uniform (38), we express the rate of de-esterification per unit volume as $k_e r_e$, where r_e is the concentration of esterified residues in the wall and k_e is a rate constant that depends on the concentration of active PME.

Proseus and Boyer (2) demonstrated that uncross-linked, de-esterified pectin is able to extract calcium from existing cross-links, thereby dissociating them (Fig. 3, Step 4). Thus, we propose that the rate of cross-link dissociation per unit volume is $k_d r_d \chi$, where r_d is the concentration of de-esterified (but not cross-linked) pectin residues, χ is the concentration of cross-links, and k_d is a rate constant. Furthermore, we propose that whenever a cross-link is dissociated, another one immediately forms due to the high affinity of de-esterified residues to bind calcium. In effect, the cross-link switches loci, exposing one of the residues from the original cross-link. The rate of cross-linking per unit volume due to this process of cross-link exchange is simply equal to the rate of cross-link dissociation, $k_d r_d \chi$.

In this light, we address the constitutive mechanical behavior of the cell wall. As load-bearing cross-links are dissociated, the network must yield to balance the turgor forces (Fig. 3, Step 5). Indeed, the growth of *Chara* cells accelerates when calcium is extracted from their walls by extracellular de-esterified pectin (2). To solve for the rheological behavior of the polymeric gel, we liken it to a network of linear elastic springs. To first order, the incremental strain of the cell wall resulting from the release of one load-bearing polymer scales as ε/χ, where ε is the strain of that polymer. Taken together with the rate of cross-link dissociation described above, this result leads to a simple expression for the strain rate of the wall,

$$\dot{\varepsilon}_i = k_d r_d \langle \varepsilon_i \rangle, \tag{1}$$

where $\langle \varepsilon_i \rangle$ is the average strain of the load-bearing polymers in the direction i. We refer to this equation as the "constitutive relation".

Like the individual polymers, the bulk material is linearly elastic and the strains are calculated from the stress-strain relationships, $\langle \varepsilon_i \rangle = 1/E\ (\sigma_i - \nu\sigma_j)$, where ν is the Poisson ratio between the orthogonal in-plane directions indexed by i and j, and the Young's modulus can be expressed in terms of the physical constants associated with the pectin gel, $E = \tilde{k}\xi\chi$, where $\tilde{k}$ is the spring constant of the polymers and ξ is the mesh size. The stresses, $\sigma_{i,j}$, are calculated from the geometry of the cell wall by balancing them with the turgor pressure, P (28) (Eq. S7 and Eq. S8 in the Supporting Material). Zerzour et al. (39) provided evidence that P is constant in time, even during oscillatory growth.

We may now return to our three guiding questions and answer them in terms of the present mechanism of wall expansion:

First, what is the constitutive rheological behavior of the cell wall? The answer, of course, is encapsulated by the constitutive relation (Eq. 1) and the stress-strain relationships. The mechanism falls under the chemorheological conception of the cell wall because irreversible deformation depends on two chemical reactions: de-esterification of pectin and cross-link dissociation.

Second, how does deposition affect the rheological properties of the wall? By combining Eq. 1 with the stress-strain relationships, we find that the effective viscosity of the wall is $\eta_{eff} = E/k_d r_d$. Thus, deposition of esterified pectin transiently increases the viscosity of the cell wall (due to dilution of the de-esterified residues) but subsequently decreases the viscosity as the pectin is de-esterified.

Third, how is mechanical thinning balanced with deposition? To address this, we note that one way to guarantee this balance is for the cell to maintain a constant area density of cross-links: $\chi_A = \chi\delta = const.$, where δ is the thickness of the cell wall. Because χ is bounded above by the total concentration of pectin residues, β, the wall thickness is bounded below by $\delta\chi = \chi_A/\beta$. That is, a discrete volume, V, of deposited wall material ultimately contributes a well-determined area, V/δ_χ, to the fully cross-linked, nonexpanding subapical wall. Conceptually, this implies that uncross-linked pectin represents a reservoir of stored material awaiting incorporation into the cross-linked portion of the wall. When this reservoir is depleted, expansion ceases. That is, according to this paradigm, wall expansion is actually limited by deposition.

The condition $\chi_A = const.$ is intriguing because, within our model, it prescribes the total rate of cross-linking per unit volume to be $k_d r_d \chi + k_d r_d \chi\ \langle \varepsilon_A \rangle$, where $\langle \varepsilon_A \rangle = \langle \varepsilon_s \rangle + \langle \varepsilon_\theta \rangle$ is the areal strain in the cell wall. The first term represents those cross-links formed through cross-link exchange whereas the second term represents those formed de novo, i.e., between two previously uncross-linked residues. Because the strain in the cell wall is around a few percent (40), the rate of de novo cross-linking (which also equals the rate at which free calcium is sequestered into the cell wall) is relatively small compared to the rate of cross-link exchange. Thus, we impose the condition $\chi_A = const.$ as a means of balancing deposition with thinning and assert that cross-link exchange is critical for this balance.

Because the condition on χ_A reduces the dynamical system by allowing us to express χ in terms of δ, the entire kinetics of pectin chemistry can be expressed in terms of the de-esterified species,

$$\dot{r}_d = \underbrace{k_e r_e}_{\text{de-esterification}} \underbrace{-2k_d r_d \langle \varepsilon_A \rangle}_{\text{cross-linking}} \underbrace{- \frac{D}{\delta} r_d}_{\substack{\text{dilution} \\ \text{by} \\ \text{deposition}}} \underbrace{- v_s \frac{\partial r_d}{\partial s}}_{\text{advection}}, \quad (2)$$

where D is the rate of deposition and v_s is the rate at which the wall material moves along cell meridians in the frame of reference of the pole of the cell (Fig. 2).

To close the model we must consider the dynamics of deposition. We posit that cell elongation downregulates deposition such that cell wall expansion and deposition check-and-balance each other as part of a negative feedback loop (Fig. 3, Step 6),

$$D \sim \alpha\left(v_{crit} - v_{pole}\right), \quad (3)$$

where v_{crit} is the elongation rate above which no deposition occurs and α is a constant of proportionality. To ensure tip growth, we confine deposition to a finite apical region, $s < a$. Yan et al. (23) described one potential mechanistic basis for the negative feedback formulated in Eq. 3 by demonstrating that cytosolic calcium, which enters the cell through stretch-activated ion channels as a result of cell wall expansion, may downregulate the polymerization of the actin cytoskeleton, the structure responsible for the delivery of secretory vesicles to the apex.

Finally, a simple continuity equation determines the thickness of the cell wall,

$$\dot{\delta} = \underbrace{D}_{\text{deposition}} \underbrace{-\delta\dot{\varepsilon}_A}_{\substack{\text{mechanical} \\ \text{thinning}}} \underbrace{-v_s \frac{\partial \delta}{\partial s}}_{\text{advection}}, \quad (4)$$

where $\dot{\varepsilon}_A$ is the areal strain rate, and we have followed previous studies (28,30) in assuming that the wall is incompressible.

To sum, the model consists of a system of partial differential equations (the closed system is given by Eq. S1, Eqs. S5–S10, and Eqs. S13 and S14 in the Supporting Material) that determines the values of three independent variables (r_d, D, and δ), each of which is a function of the arclength, s, and of time. Additionally, the position of the cell wall is itself variable in time. From these variables, all other quantities, such as the strain rates and the cross-link concentration,

can be solved for. Despite the sophistication of the model, there are only three nondimensional free parameters that determine its behavior (Table 1).

RESULTS

The strains in the cell wall predict its strain rates

Our constitutive relation accounts for data reported by Métraux and Taiz (41), which shows a linear relationship between the strain and the strain rate in the walls of the diffusely growing alga *Nitella axillaris*. To test the constitutive relation within pollen tubes, we made precise measurements of the morphology and strain rate profiles of steady cells and compared them to solutions of the model within the steady regime. To measure the morphology, we captured bright-field time-lapse image sequences of growing pollen tubes (see Movie S1 in the Supporting Material) from which we extracted the time-dependent position of the cell wall (Fig. 4 *A*; see Materials and Methods in the Supporting Material). The time-averaged curvature of a cell meridian, $\kappa_s(s) = \partial\varphi/\partial s$, gives a precise quantification of cell morphology (Fig. 4 *B*), where $\varphi(s)$ is the angle between a vector normal to the cell surface and the cell axis (Fig. 2).

Strain rates within a flowing material may be expressed in terms of the gradient of the velocity field. Thus, to measure the strain rates within the cell wall we attached fluorescent microspheres to it and tracked their movement from simultaneously recorded bright-field and epifluorescence time-lapse image sequences (Fig. 4 *C*, see Movie S1 and Movie S3). In the frame of reference of the pole of the cell, the microspheres travel along cell meridians at the meridional velocity, $v_s(s)$ (Fig. 4 *D*). We performed a free fit of $v_s(s)$ whereby the number of free parameters was unconstrained except by the degree of precision of the data (42) (see the Supporting Material for details). From the experimental curvature profile (Fig. 4 *B*) and the free fit of $v_s(s)$, the spatial profiles of the principal strain rates can be calculated (Fig. 4 *E*; and see Eq. S11 and Eq. S12 in the Supporting Material for the formulas). Additionally, the principal stresses can be estimated by assuming a uniform wall thickness (Fig. 4 *E*; and see Eq. S7 and Eq. S8 in the Supporting Material).

Based on the physical parameters given in Table 1, we searched what we determined to be a physically realistic region of the model's parameter space and obtained an excellent fit of the experimentally measured meridional velocity profile (see Fig. S3). The close agreement of the principal strain rates calculated from this fit (Fig. 4 *F*) with those calculated from the free fit (Fig. 4 *E*) gives us additional confidence in the accuracy of the former, particularly because the strain rates are calculated from the derivatives of the fits, which would tend to accentuate discrepancies between the two.

The strain rate profiles from both the data and the model feature characteristic circumferential strain-rate anisotropy ($\dot{\varepsilon}_\theta > 0\dot{\varepsilon}_s$) throughout the expanding cell wall, except for at the pole, where the principal strain rates are necessarily equal due to symmetry. The model also captures the curious negative strain rates in the meridional direction ($\dot{\varepsilon}_s < 0$) observed near the base of the cell apex, a phenomenon previously observed in root hairs (42). Both of these phenomena are manifestations of circumferential stress anisotropy ($\sigma_\theta > \sigma_s$, Fig. 4 *E*). The negative meridional strain rates are due to a Poisson effect—significant circumferential stress anisotropy causes contraction in the meridional direction, according to the stress-strain relationships. This contraction (negative strain) is translated into a negative strain rate per the constitutive relation. Because the morphology is well determined by the principal strain rate profiles (but not vice versa), a close fit of the latter automatically yields an accurate prediction for the former (Fig. 4 *B*). The agreement between the model and the data was consistent across the four cells analyzed (see Fig. S3 and Fig. S4).

Finally, as a direct result of the linear scaling between the principal strain rates and the principal strains, the strain rate anisotropy, defined as $\gamma_{\dot{\varepsilon}} = (\dot{\varepsilon}_\theta - \dot{\varepsilon}_s)/\dot{\varepsilon}_\theta$, should equal the

TABLE 1 Parameters upon which the parameter space search was based

Parameter	Symbol	Value	Reference
ND rate constant for cross-link dissociation.	$k^*_d = Pk_d/2k_e\xi\tilde{k}$	0.009	N/A
ND critical elongation rate.	$\nu^*_{crit} = \beta\nu_{crit}/\chi_A k_e$	172	N/A
Dependence of deposition on elongation rate.	α	0.19	*
Poisson ratio.	ν	0.78	*
ND length scale over which exocytosis occurs.	$a^* = \beta_d/\chi_A$	75	N/A
Turgor pressure.	P	2 atm	(45)
Mesh size.	ξ	5 nm	(46)
Concentration of pectin residues.	β	88.9 mM	(47)*
Intrinsic spring coefficient of pectin.	$\tilde{k}$	2 nN	(48)*
Rate constant for de-esterification.	k_e	0.024 s^{-1}	*
Critical velocity.	ν_{crit}	0.41 μm/s	*
Rate constant for cross-link dissociation.	k_d	0.014 m^3/mol−s	*
Area density of cross-links.	χ_A	8.9 μmol/m^2	(49)*
Arclength over which exocytosis occurs.	a	7.5 μm	(50)

First five parameters are the independent, nondimensional (ND) parameters. The first three nondimensional parameters are the free parameters that were used to study the behavior of the system. The Poisson ratio is independently constrained by the strain rate measurements while a^* sets the size of the simulated cells.

*Values of the physical parameters were either obtained from the literature or calculated empirically in this study (denoted *, see Table S2 in the Supporting Material for calculations).

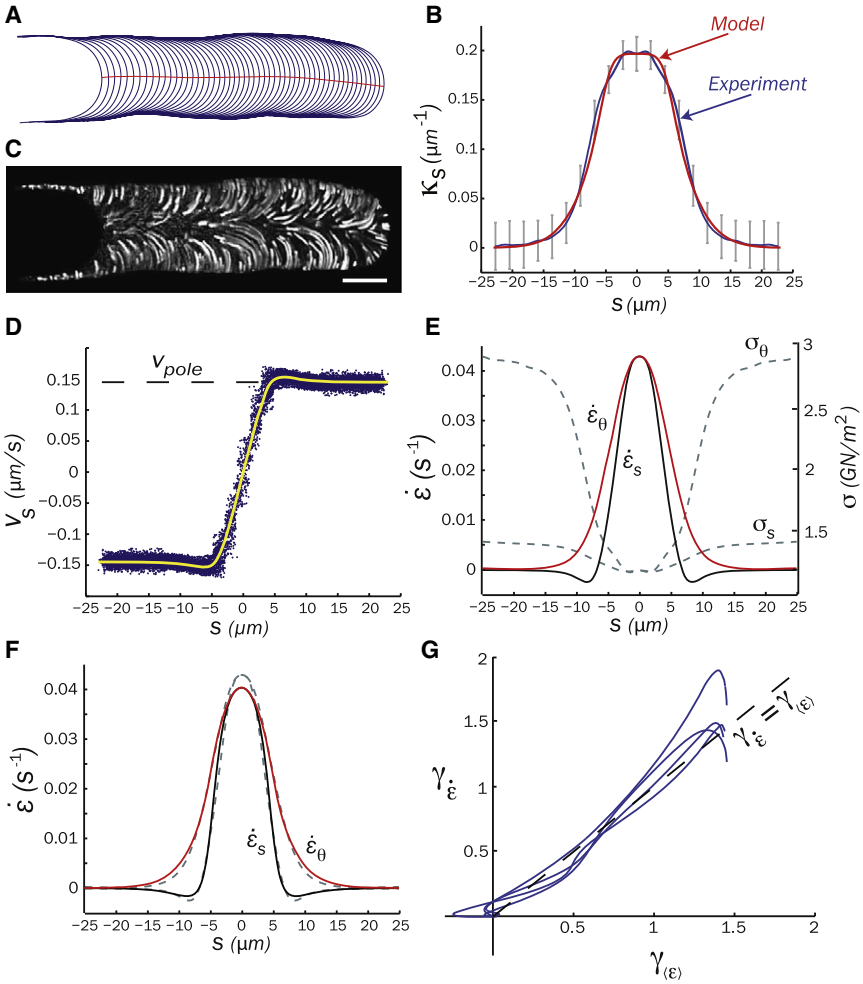

FIGURE 4 We measured the morphology of steady cells and the deformation rates of their cell walls. (*A*) The position of the cell wall was tracked from a bright-field image sequence. (*B*) The time-averaged curvature of a cell meridian, $\kappa_s(s)$, gives a quantification of the morphology. The error bars represent $\pm$ 1 SD. (*C*) The kinematics of the cell wall were measured by attaching fluorescent microspheres to the cell wall (Scale bar = 5 μm). (*D*) We performed an empirical, free fit of the v_s data (*yellow line*). (*E*) The principal strain rates are calculated from this fit. The principal stresses are calculated from the geometry of the cell wall. To calculate the stresses shown here, we assumed a uniform thickness, $\delta = 0.1$ μm. (*F*) The best fit of the meridional velocity profile by our model yields strain rate profiles that are in excellent agreement with the empirical profiles (*dotted lines* are the same empirical strain rates shown in panel *E*). (*G*) The model correctly predicts that the strain rate anisotropy, $\gamma_{\dot{\varepsilon}}$, equals the strain anisotropy, $\gamma_{\langle\varepsilon\rangle}$, for each of the four cells.

strain anisotropy, $\gamma_{\langle\varepsilon\rangle} = (\langle\varepsilon_\theta\rangle - \langle\varepsilon_s\rangle)/\langle\varepsilon_\theta\rangle$, regardless of k_d or r_d. This is a stringent prediction: first, nonlinear scaling or absence of scaling between $\dot{\varepsilon}_i$ and $\langle\varepsilon_i\rangle$ would not yield this equality; second, the only fitting parameter is the Poisson ratio with which $\gamma_{\langle\varepsilon\rangle}$ is calculated using the stress-strain relationships. A single Poisson ratio, $\nu = 0.78$, yields an excellent fit for all four cells (Fig. 4 *G*).

By validating the linear scaling between the strain rates and the strains while also fitting the strain rate profiles, we implicitly demonstrate the ability of Eq. 1 to explain the spatial profile of wall rheological properties ($g(s) = E/\eta_{eff} = k_d r_d$) through the profile of the de-esterified pectin concentration.

Rapidly growing cells have oscillatory growth rates

The model has both steady-state and periodic solutions and thus correctly predicts steady and oscillatory cell growth (Fig. 5, *A–C*). The surface in parameter space that separates the two regimes can be closely approximated by the plane $v_{avg}/v_{crit} \approx 0.7$ (Fig. 5 *A*), where v_{avg} is the average elongation rate. The tacit prediction is that there is a threshold elongation rate above which a given cell will oscillate. Although experimentally we cannot control v_{crit} or the various intrinsic parameters that set v_{avg}, if we consider a large number of cells we expect that faster ones are more likely to oscillate. Indeed, this is the case (Fig. 5 *D*). In light of the model presented here, this suggests a simple paradigm for oscillatory growth: that when the rate of elongation is large enough, the cell essentially outruns sufficient deposition. Because expansion is rate-limited by deposition—a proposition that relies on the idea of cross-link exchange—the cell decelerates when deposition is significantly attenuated. In the subsequent slow phase of growth, material is deposited in excess. Another phase of rapid expansion occurs as this material is de-esterified. Thus, the elongation rate dependence of oscillatory behavior is consistent with the ideas of cross-link exchange and deposition-induced cross-link dissociation.

Deposition is out of phase with elongation rate

Although it is not currently possible to measure the rate of deposition directly, we can estimate it by performing a mass-balance calculation. Having measured the strain rate

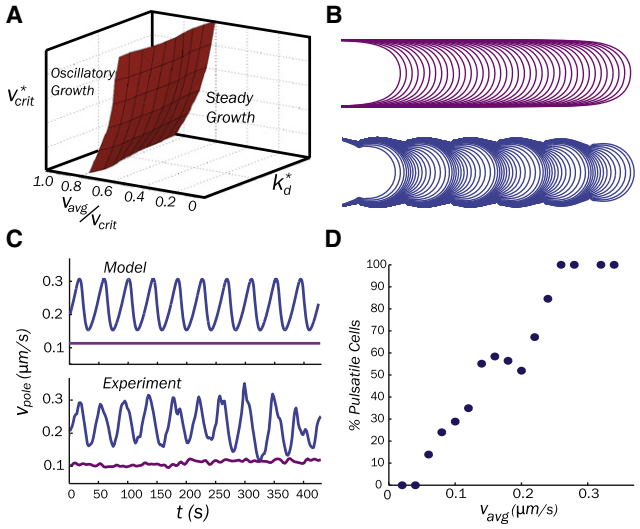

FIGURE 5 Behavior of the model compares well with the experimental behavior of pollen tubes. (*A*) The state space of the model has steady and oscillatory regimes. Simulations of cell growth show the two behaviors with distinct (*B*) morphologies and (*C*) elongation rate traces. (*D*) Inspecting the percentage of cells that are oscillatory at each mean elongation rate verifies that faster cells are more likely to oscillate ($n = 101$).

profiles of several steady cells, we find that the polar strain rate is related to the elongation rate by the expression $\dot{\varepsilon}_{pole} = 1.73 v_{pole}/R$, where R is the cell radius (see the Supporting Material). If we apply this analysis to data reported by McKenna et al. (10), who give simultaneous measurements of the elongation rate and the polar thickness of the cell wall of an oscillatory cell, we can solve Eq. 4 to find the rate of deposition at its pole. This calculation shows deposition to be approximately out-of-phase with the elongation rate and supports the scaling given in Eq. 3 (see Fig. S2).

The model explains oscillatory morphology

Oscillatory cells can be characterized according to their elongation rates and their morphologies. The scaled wavelength, $\bar{\lambda} = v_{avg}T/R$ (Fig. 6 *A*, where T is the period of oscillation), is a useful geometrical scalar that can be calculated from these data. Because $\bar{\lambda}$ is nondimensional, by fitting it with the model we fit the relative values of a milieu of variables (v_{avg}, T, and R) without directly relying on the values that we assign to the physical parameters. Experimentally, we observed a range of scaled wavelengths between 0.8 and 2 (Fig. 6 *B*), though the distribution was tightly confined around the mean, $\bar{\lambda} = 1.2$. The distribution of $\bar{\lambda}$ yielded by solutions of the model within the physical range of parameter space agrees with the experimental distribution (Fig. 6 *B*).

The apparent selection rule, $\bar{\lambda} \approx 1$, can be understood by appealing to the prediction that $\delta_\chi = const.$ It can be shown that the volume of stored (uncross-linked) material present during the slow phase of growth, V, sets the radius of the cell through δ_χ: $R^2 \approx V/2\pi\delta_\chi$ (see the Supporting Material for derivation). Also, during one oscillatory cycle, the length of the subapical region increases by $\lambda \approx V/2\pi R\delta_\chi$. Combining these expressions yields $\bar{\lambda} \approx 1$. The experimental agreement of this scaling argument supports the idea of cross-link exchange, upon which the condition $\delta_\chi = const.$ relies.

The scaled wavelength reflects the more complex pearled morphology of oscillatory cells (Fig. 6, *A*, *C*, and *D*). Each of the 20 cells we analyzed showed pearling to a greater or lesser extent, as evidenced by opposing rays on three-dimensional (κ_s, s, t) plots (Fig. 6 *E*). A bulge in radius appears first as a strong peak in curvature at or near the pole. The bulge is then translated away from the pole and is set into place permanently as it enters the nonexpanding region of the cell wall. Cells simulated by the model share these qualitative features (Fig. 5 *B* and Fig. 6 *F*).

To produce the pearled morphology, it is clear that the apical geometry oscillates. This notion prompted us to inspect the limit cycle in the (v_{pole}, κ_{pole}) phase space, where $\kappa_{pole} = \kappa_s(0)$. The model can fit a variety of experimental limit cycles, most of which share some salient characteristics, such as clockwise trajectories (Fig. 6 *G* and see Fig. S6).

The pearled morphology results from the fact that deposition and expansion are not precisely coordinated in space. In the Discussion and Conclusions, we give a detailed interpretation of pearling in terms of our model by additionally considering oscillations of the wall thickness.

Wall thickness anticipates elongation rate

In lily pollen tubes, oscillations of the apical cell wall thickness, $\delta_{pole} = \delta(0)$, precede those of the elongation rate by between 74° and 130°, with an average phase of $\phi_\delta = 99°$ (in tobacco pollen tubes, the average phase is 124°) (13). Within the physical range of parameter space, the model yields a distribution of ϕ_δ between 90° and 142° (e.g., Fig. 6 *H*; see Fig. S7 for distribution).

That wall-thickening precedes periods of rapid expansion would be puzzling if thickening acted to curb expansion. However, this observation is consistent with the role of deposition to transiently loosen the cell wall via dissociation of cross-links. Moreover, expansion subsides not when the wall thickens, but when most of the available de-esterified pectin has been incorporated into the load-bearing wall, i.e., when the wall thins. Thus, like the elongation rate dependence of oscillatory cells (Fig. 5 *D*), measurements of ϕ_δ are consistent with the prediction that expansion is rate-limited by deposition and the idea of cross-link exchange.

DISCUSSION AND CONCLUSIONS

In this article, we have provided a simple model of pectic wall expansion that can account for several phenomena in

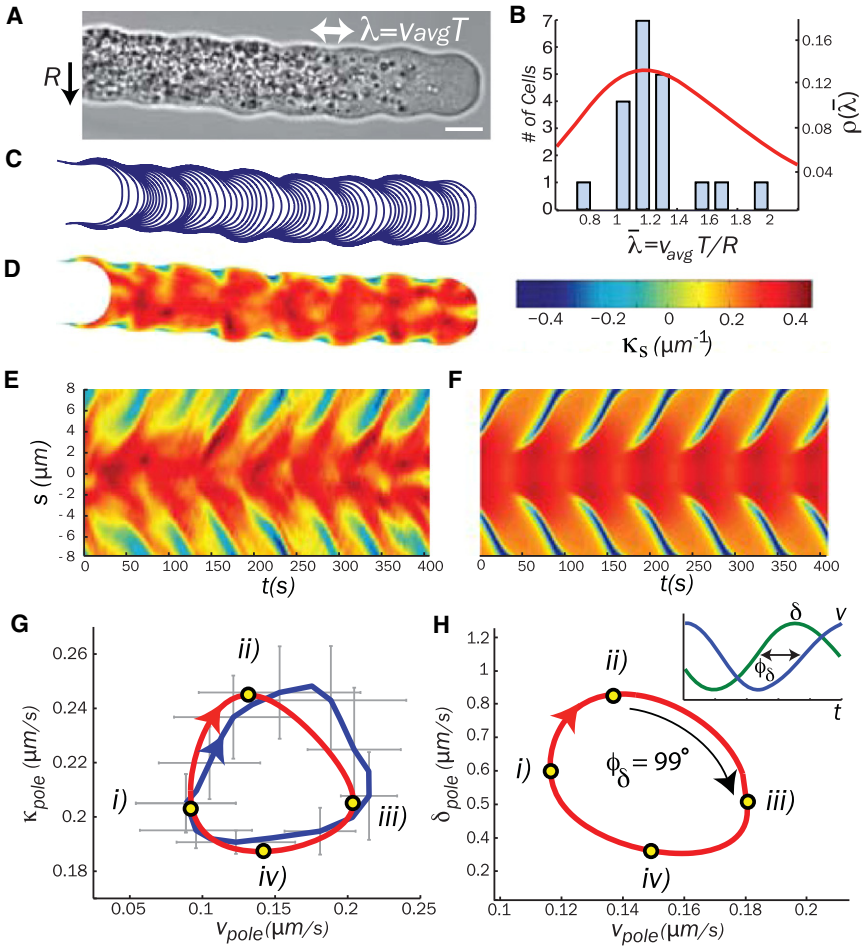

FIGURE 6 We examined several morphological aspects of oscillatory cells. (*A* and *B*) The scaled wavelength, $\bar{\lambda}$, captures a breadth of information from the (*C*) time-dependent position of the cell wall (Scale bar = 5 μm). (*B*) A histogram shows that cells select $\bar{\lambda} \approx 1$, as does the distribution of $\bar{\lambda}$ yielded by solutions of the model (*red line*), where $\rho(\bar{\lambda})$ is the probability density in parameter space for a simulated cell to have scaled wavelength $\bar{\lambda}$. (*A* and *C*) The pearled morphology can be visualized by (*D*) mapping the curvature of the cell wall onto its position or with a (*E*) three-dimensional (κ_s, s, t) graph. (*F*) The morphology of simulated cells shows qualitative agreement with the data. (*G*) Experimental limit cycles in (v_{pole}, κ_{pole}) phase space (e.g., *blue line*; error bars represent $\pm$ 1 SD) can be fit with those scribed by simulated cells (*red line*). (*H*) In simulated cells, as in the data, oscillations in the thickness of the apical cell wall, δ_{pole}, precede those of the elongation rate. We chose the fitting parameters here such that the time dependence of v_{pole} and δ_{pole} (*inset*) most closely resembles the data concerning the phase of thickness published by McKenna et al. (10).

pollen tubes. The model is based on three key concepts: i), that cross-link dissociation allows turgor forces to stretch the cell wall, thereby determining its rheological behavior; ii), that deposition actively induces dissociation of cross-links; and iii), that cross-links immediately reform after they are dissociated, which contributes to a cell's ability to balance deposition with mechanical thinning.

Additionally, the model provides a mechanistic explanation for the aforementioned stored-growth phenomenon (6–9). In effect, temporary plasmolysis of a plant cell creates an artificial oscillatory cycle; the extent of deposition during plasmolysis determines the ultimate length of the cell, while turgor is needed to facilitate expansion.

Oscillatory pollen tubes provide an excellent demonstration of the relationship between deposition and mechanics according to our model. By examining the (v_{pole}, κ_{pole}) and (v_{pole}, δ_{pole}) limit cycles (Fig. 6, *G* and *H*) in tandem, we can reillustrate the feedback cycle presented in Fig. 2 in terms of oscillatory pollen tube phenomenology, as follows (Fig. 7):

1. During the phase of slowest elongation, deposition is highest and takes place over a well-defined area. The wall thickens and material is stored in this area.
2. The phase of maximum thickness coincides with the phase of acceleration, as the stored material is de-esterified. Expansion initially occurs over the same area as

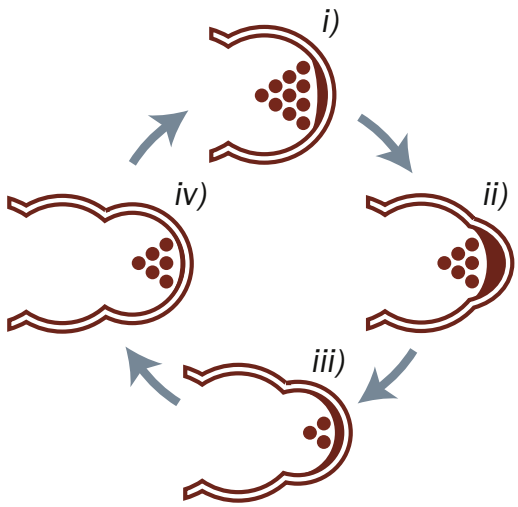

FIGURE 7 Illustration of the temporal relationship between κ_{pole} and δ_{pole} elucidates the origin of the pearled morphology. The number of vesicles (*dark circles*) represents the rate of deposition.

deposition. Because the pole curvature is inversely correlated with the area over which the cell wall is expanding (smaller cells have higher curvatures), the cell becomes tapered (κ_s increases) during this phase.

3. During the phase of fastest elongation, deposition is lowest, the cell-wall thins markedly due to mechanical expansion, and the stored material that is not yet incorporated into the load-bearing wall becomes distributed over a wider area. As a result, expansion takes place over a wider area and the cell becomes oblate (κ_s decreases).
4. As the stored material is exhausted, the wall reaches its thinnest point, and the cell decelerates. Because expansion is still occurring over a wide area, the cell becomes increasingly oblate during this phase.

In principle, oscillatory tip growth does not lead inevitably to a pearled morphology (28). It is because the area over which expansion occurs also oscillates that this shape is obtained. Our model elucidates this phenomenon per the above interpretation of an oscillatory cycle.

In addition to those of curvature and thickness, we can explain oscillations in the apical cytosolic calcium concentration, which lag those in the growth rate by $\approx 38^\circ$ (17), by formulating calcium influx through stretch-activated ion channels and solving for diffusion in the cytosol (see Fig. S8 and a discussion in the Supporting Material). Previous models of oscillations in pollen tubes have postulated different roles for calcium: 1), that it determines the rate of deposition (31,32); or 2), that it feeds-back negatively to growth by down-regulating either actin assembly or the ROP1 GTPase, a morphogen known to determine polarity (23). The second model, which considers only oscillations in solute concentrations but not those in the growth rate, is consistent with ours and it may be possible to couple the two models via the calcium concentration to obtain a mechanistic description of the negative feedback between growth and deposition encompassed by Eq. 3. Models of other ionic oscillators (e.g., CI^-, H^+) (43) may perhaps be coupled to our model similarly.

Future models should also address the full system of chemical kinetics that determines pollen tube morphogenesis. Specifically, our model lacks a mechanistic formulation of de novo cross-linking. This could account for the apparent discrepancy between studies that suggest a growth-promoting effect of de-esterified pectin (ours and one by Proseus and Boyer (2)) and those that show an inhibitory effect of exogenous PME (38,44) as well as a growth-promoting effect of the PME inhibitor, PMEI (38). Having derived the rate of de novo cross-linking from the stability condition, $\chi_A = const.$, we preclude, for example, a thick, fully cross-linked, rigid wall like that which probably forms when the cell is flooded with nonphysiological amounts of PME. In reality, our model may represent one limit of a complex dynamical system that involves the concentrations of PME and PMEI. A chemical kinetics-based treatment of cross-linking needs to be formulated to test these ideas and to further elucidate the mechanisms of dynamical stability in cell growth.

Finally, although this study only deals with the pectic phase of the cell wall, the mechanism we have presented in this article has clear implications for plant cells whose walls also contain cellulose. Future studies should consider the behavior of the pectic phase in parallel with the cellulose-hemicellulose network to provide a unified model of plant cell wall expansion.

SUPPORTING MATERIAL

Additional theory and narrative with Materials and Methods, seven figures, two tables, supporting equations, and three movies are available at http://www.biophysj.org/biophysj/supplemental/S0006-3495(11)00962-3.

We thank Arezki Boudaoud for insightful comments concerning the manuscript.

This work was partially supported by a National Science Foundation-Integrative Graduate Education and Research Traineeship Biomechanics Training Grant at Harvard University and by the Human Frontier Science Program.

REFERENCES

1. Ray, P. M., and A. W. Ruesink. 1962. Kinetic experiments on the nature of the growth mechanism in oat coleoptile cells. *Dev. Biol.* 4:377–397.
2. Proseus, T. E., and J. S. Boyer. 2006. Calcium pectate chemistry controls growth rate of *Chara corallina*. *J. Exp. Bot.* 57:3989–4002.
3. Baskin, T. I. 2005. Anisotropic expansion of the plant cell wall. *Annu. Rev. Cell Dev. Biol.* 21:203–222.
4. Schindler, T., R. Bergfeld, …, P. Schopfer. 1994. Inhibition of Golgi-apparatus function by brefeldin A in maize coleoptiles and its consequences on auxin-mediated growth, cell-wall extensibility and secretion of cell-wall proteins. *Planta.* 192:404–413.
5. Wang, Q., L. Kong, …, F. Baluska. 2005. Effects of brefeldin A on pollen germination and tube growth. Antagonistic effects on endocytosis and secretion. *Plant Physiol.* 139:1692–1703.
6. Ray, P. M. 1961. Hormonal regulation of plant cell growth. *In* Control Mechanisms in Cellular Processes. D. M. Bonner, editor. Ronald Press, New York. 185–212.
7. Acevedo, E., T. C. Hsiao, and D. W. Henderson. 1971. Immediate and subsequent growth responses of maize leaves to changes in water status. *Plant Physiol.* 48:631–636.
8. Cosgrove, D. J. 1987. Wall relaxation in growing stems: comparison of four species and assessment of measurement techniques. *Planta.* 171:266–278.
9. Proseus, T. E., and J. S. Boyer. 2008. Calcium pectate chemistry causes growth to be stored in *Chara corallina*: a test of the pectate cycle. *Plant Cell Environ.* 31:1147–1155.
10. McKenna, S. T., J. G. Kunkel, …, P. K. Hepler. 2009. Exocytosis precedes and predicts the increase in growth in oscillating pollen tubes. *Plant Cell.* 21:3026–3040.
11. Schröter, K., and A. Sievers. 1971. Effect of turgor reduction on the Golgi apparatus and the cell wall formation in root hairs. *Protoplasma.* 72:203–211.
12. Pierson, E. S., Y. Q. Li, …, M. Cresti. 1995. Pulsatory growth of pollen tubes: investigation of a possible relationship with the periodic distribution of cell wall components. *Acta Bot. Neerl.* 44:121–128.

13. Pierson, E. S., D. D. Miller, …, P. K. Hepler. 1996. Tip-localized calcium entry fluctuates during pollen tube growth. *Dev. Biol.* 174:160–173.

14. Hwang, J.-U., Y. Gu, …, Z. Yang. 2005. Oscillatory ROP GTPase activation leads the oscillatory polarized growth of pollen tubes. *Mol. Biol. Cell.* 16:5385–5399.

15. Cárdenas, L., S. T. McKenna, …, P. K. Hepler. 2006. NAD(P)H oscillates in pollen tubes and is correlated with tip growth. *Plant Physiol.* 142:1460–1468.

16. Holdaway-Clark, T. L., J. A. Feijó, …, P. K. Hepler. 1996. Pollen tube growth and the intracellular cytosolic calcium gradient oscillate in phase while extracellular calcium influx is delayed. *Plant Cell.* 9:1999–2010.

17. Messerli, M. A., R. Créton, …, K. R. Robinson. 2000. Periodic increases in elongation rate precede increases in cytosolic Ca^{2+} during pollen tube growth. *Dev. Biol.* 222:84–98.

18. Ferguson, C., T. T. Teeri, …, A. Bacic. 1998. Location of cellulose and callose in pollen tubes and grains of *Nicotiana tabacum*. *Planta.* 206:452–460.

19. Miller, D. D., S. P. Scordilis, and P. K. Hepler. 1995. Identification and localization of three classes of myosins in pollen tubes of *Lilium longiflorum* and *Nicotiana alata*. *J. Cell Sci.* 108:2549–2563.

20. Lovy-Wheeler, A., K. L. Wilsen, …, P. K. Hepler. 2005. Enhanced fixation reveals the apical cortical fringe of actin filaments as a consistent feature of the pollen tube. *Planta.* 221:95–104.

21. Cheung, A. Y., S. Niroomand, …, H. M. Wu. 2010. A transmembrane formin nucleates subapical actin assembly and controls tip-focused growth in pollen tubes. *Proc. Natl. Acad. Sci. USA.* 107:16390–16395.

22. Kroeger, J. H., F. B. Daher, …, A. Geitmann. 2009. Microfilament orientation constrains vesicle flow and spatial distribution in growing pollen tubes. *Biophys. J.* 97:1822–1831.

23. Yan, A., G. Xu, and Z.-B. Yang. 2009. Calcium participates in feedback regulation of the oscillating ROP1 ρ-GTPase in pollen tubes. *Proc. Natl. Acad. Sci. USA.* 106:22002–22007.

24. Schols, H. K., and A. G. J. Voragen. 2002. The chemical structure of pectins. *In* Pectins and Their Manipulation. G. P. Seymour and J. P. Knox, editors. Blackwell Publishing, CRC Press, Oxford, UK. 1–29.

25. Storm, C., J. J. Pastore, …, P. A. Janmey. 2005. Nonlinear elasticity in biological gels. *Nature.* 435:191–194.

26. Bartnicki-Garcia, S., F. Hergert, and G. Gierz. 1989. Computer simulation of fungal morphogenesis and the mathematical basis for hyphal (tip) growth. *Protoplasma.* 153:46–57.

27. Goriely, A., and M. Tabor. 2003. Self-similar tip growth in filamentary organisms. *Phys. Rev. Lett.* 90:108101.

28. Dumais, J., S. L. Shaw, …, P. M. Ray. 2006. An anisotropic-viscoplastic model of plant cell morphogenesis by tip growth. *Int. J. Dev. Biol.* 50:209–222.

29. Fayant, P., O. Girlanda, …, A. Geitmann. 2010. Finite element model of polar growth in pollen tubes. *Plant Cell.* 22:2579–2593.

30. Campàs, O., and L. Mahadevan. 2009. Shape and dynamics of tip-growing cells. *Curr. Biol.* 19:2102–2107.

31. Kroeger, J. H., A. Geitmann, and M. Grant. 2008. Model for calcium dependent oscillatory growth in pollen tubes. *J. Theor. Biol.* 253:363–374.

32. Kroeger, J. H., R. Zerzour, and A. Geitmann. 2011. Regulator or driving force? The role of turgor pressure in oscillatory plant cell growth. *PLoS ONE.* 6:e18549.

33. Lockhart, J. A. 1965. An analysis of irreversible plant cell elongation. *J. Theor. Biol.* 8:264–275.

34. Passioura, J. B., and S. C. Fry. 1992. Turgor and cell expansion: beyond the Lockhart equation. *Aust. J. Plant Physiol.* 19:565–576.

35. Bosch, M., and P. K. Hepler. 2005. Pectin methylesterases and pectin dynamics in pollen tubes. *Plant Cell.* 17:3219–3226.

36. Li, Y. Q., F. Chen, …, M. Cresti. 1994. Distribution of unesterified and esterified pectins in cell walls of pollen tubes of flowering plants. *Sex. Plant Reprod.* 7:145–152.

37. Parre, E., and A. Geitmann. 2005. Pectin and the role of the physical properties of the cell wall in pollen tube growth of *Solanum chacoense*. *Planta.* 220:582–592.

38. Röckel, N., S. Wolf, …, S. Greiner. 2008. Elaborate spatial patterning of cell-wall PME and PMEI at the pollen tube tip involves PMEI endocytosis, and reflects the distribution of esterified and de-esterified pectins. *Plant J.* 53:133–143.

39. Zerzour, R., J. Kroeger, and A. Geitmann. 2009. Polar growth in pollen tubes is associated with spatially confined dynamic changes in cell mechanical properties. *Dev. Biol.* 334:437–446.

40. Proseus, T. E., J. K. E. Ortega, and J. S. Boyer. 1999. Separating growth from elastic deformation during cell enlargement. *Plant Physiol.* 119:775–784.

41. Métraux, J.-P., and L. Taiz. 1978. Transverse viscoelastic extension in *Nitella*: I. Relationship to growth rate. *Plant Physiol.* 61:135–138.

42. Dumais, J., S. R. Long, and S. L. Shaw. 2004. The mechanics of surface expansion anisotropy in *Medicago truncatula* root hairs. *Plant Physiol.* 136:3266–3275.

43. Liu, J., B. M. Piette, …, P. J. Hussey. 2010. A compartmental model analysis of integrative and self-regulatory ion dynamics in pollen tube growth. *PLoS ONE.* 5:e13157.

44. Bosch, M., A. Y. Cheung, and P. K. Hepler. 2005. Pectin methylesterase, a regulator of pollen tube growth. *Plant Physiol.* 138:1334–1346.

45. Benkert, R., G. Obermeyer, and F.-W. Bentrup. 1997. The turgor pressure of growing lily pollen tubes. *Protoplasma.* 198:1–8.

46. Proseus, T. E., and J. S. Boyer. 2005. Turgor pressure moves polysaccharides into growing cell walls of *Chara corallina*. *Ann. Bot. (Lond.).* 95:967–979.

47. Yi-Qin, L., and H. F. Linskens. 1983. Neutral sugar composition of pollen tube walls of *Lilium longiflorum*. *Acta Bot. Neerl.* 32:437–445.

48. Jarvis, M. C. 2002. Biophysical properties of pectins. *In* Pectins and Their Manipulation. G. P. Seymour and J. P. Knox, editors. Blackwell Press, CRC Publishing, Oxford, UK, and Sheffield Academic Press, Sheffield, UK. 99–130.

49. Lancelle, S. A., M. Cresti, and P. K. Hepler. 1997. Growth inhibition and recovery in freeze-substituted *Lilium longiflorum* pollen tubes: structural effects of caffeine. *Protoplasma.* 196:21–33.

50. Bove, J., B. Vaillancourt, …, A. Geitmann. 2008. Magnitude and direction of vesicle dynamics in growing pollen tubes using spatiotemporal image correlation spectroscopy and fluorescence recovery after photobleaching. *Plant Physiol.* 147:1646–1658.